UNIVERSITY OF MISKOLC
FACULTY OF MECHANICAL ENGINEERING AND INFORMATICS

LATHE CHATTER PREVENTION BY SPINDLE SYSTEM STRUCTURAL MODIFICATIONS

Booklet of PhD Theses

ISTVÁN SÁLYI DOCTORAL SCHOOL OF MECHANICAL ENGINEERING SCIENCES

DESIGN MACHINES AND STRUCTURES
DYNAMICS AND STABILITY OF MACHINE TOOLS

Head of Doctoral School

Dr. Gabriella Bognár

DSc., Professor

Scientific Supervisors

Dr. Ferenc Sarka
Associate Professor

Dr. Ferenc János Szabó
Associate Professor

Dr. Attila Szilágyi
Associate Professor

Prepared by:
Mohammad Jehad Mohammad Alzghoul
IM04C8

Miskolc

2025

JUDGING COMMITTEE

Chair:

Secretary:

Members:

OFFICIAL REVIEWERS

1 INTRODUCTION

Chatter is a critical issue in machining. It arises from unstable interactions between the cutting tool and the workpiece, leading to detrimental vibrations. While most research focuses on cutting tool-based solutions, limited attention has been given to spindle system modifications in turning. This study aims to optimize a lathe spindle system to mitigate chatter while maintaining structural integrity under static loads. By implementing structural modifications, the research enhances the dynamic performance of spindle by reducing chatter occurrence.

1.1 Background

Chatter negatively impacts machining by reducing accuracy, causing poor surface finish, increasing tool wear, high noise, and wasting energy. As machining operations expand, the likelihood of chatter rises, necessitating further research to develop effective mitigation strategies. The increasing number of studies on chatter over the years, as illustrated in Figure 1, highlights a growing academic interest in understanding and addressing this issue. [1].

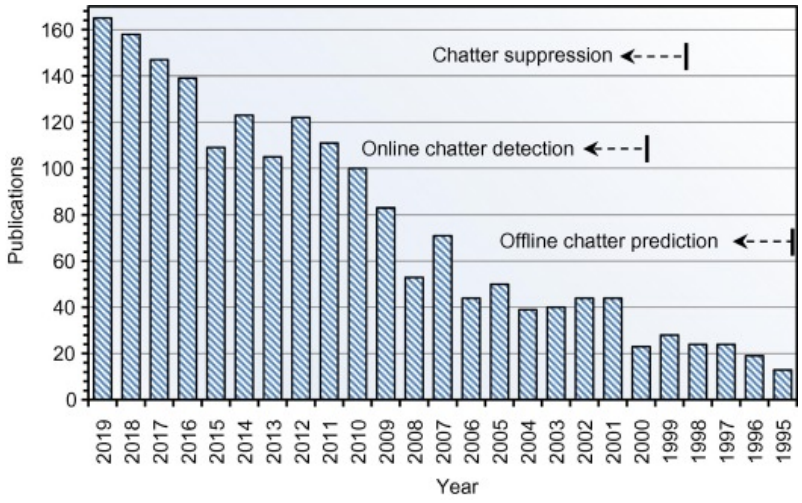

Figure 1. Trend of Chatter Publications Over Time [1].

1.2 Research Aim and Objectives

Considering the limited research on optimizing spindle system design to reduce or avoid chatter in turning, this study aims to address this gap by presenting a case study. The focus is on optimizing a spindle of lathe machine system using two distinct methods to minimize chatter occurrence. Importantly, the study ensures that the structural integrity of the spindle system remains unchanged throughout the optimization process. The objectives of this research can be summarized as follows:

a. To identify the most suitable theory or method for analysing a lathe spindle system.
b. To investigate the impact of altering dimensions such as the dimensions of the shaft of the spindle, rear bearing (which is placed farther from the chuck) location on the behaviour of the system.
c. To optimize the spindle system using the RSM (Response Surface Methodology).
d. To optimize the spindle system using the Kuhn-Tucker optimality criterion, employing the Grapho-Analytical technique.
e. To compare the optimization results obtained from the two optimization techniques.

1.3 The Importance of the Research

This research is crucial in machining as it addresses the gap in optimizing spindle system design to reduce chatter in turning. By improving machining efficiency, minimizing tool wear, and enhancing part quality, it offers practical industry benefits, including cost savings and increased competitiveness. The findings guide future studies, support industry best practices, and promote the adoption of optimized spindle systems, contributing to overall productivity and technological advancement. Additionally, the generalizability of the research ensures its applicability across various machine tools, making it a valuable resource for improving spindle design and machining performance.

2 PROPOSED MODELS AND ANALYSIS

This chapter presents a detailed analysis of two spindle systems utilizing distinct theoretical frameworks: the Euler-Bernoulli beam theory for the first system and the Timoshenko beam theory for the second. The simpler Euler-Bernoulli model lays the groundwork for advancing to a more intricate spindle system aimed at optimization. The study assesses various variables influencing the performance and behavior of the spindle under diverse conditions, thereby providing a systematic exploration of spindle dynamics that can lead to design enhancements.

2.1 Spindle Model One: Euler-Bernoulli Beam Theory

This part aims to perform dynamic simulations on a simply supported Euler-Bernoulli beam with an overhanging mass. The goal is to derive a general expression for calculating the natural frequencies and plotting the mode shapes of the system with varying configurations, such as different beam lengths, second support locations, and overhang mass values (representing the spindle chuck mass). The expression is derived using Euler-Bernoulli beam theory and Newton's second law. Figure 2 shows a pinned-pinned-free beam with an overhang and a mass

(m) attached to the free end, with the beam assumed to be slender and subjected to a transverse load (w).

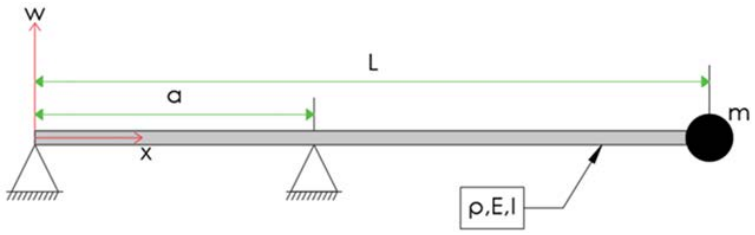

Figure 2. Pinned-Pinned-Free beam with a mass attached to the free end.

Using Euler-Bernoulli's beam theory the governing equation can be rewritten as:

$$\boldsymbol{EI\frac{\partial^4 w}{\partial x^4}(x,t)+\rho A\frac{\partial^2 w}{\partial t^2}(x,t)=0} \tag{2.1}$$

The following flow chart shows the procedure to calculate the beam vibration eigenvalues which are required to calculate the beam natural frequencies.

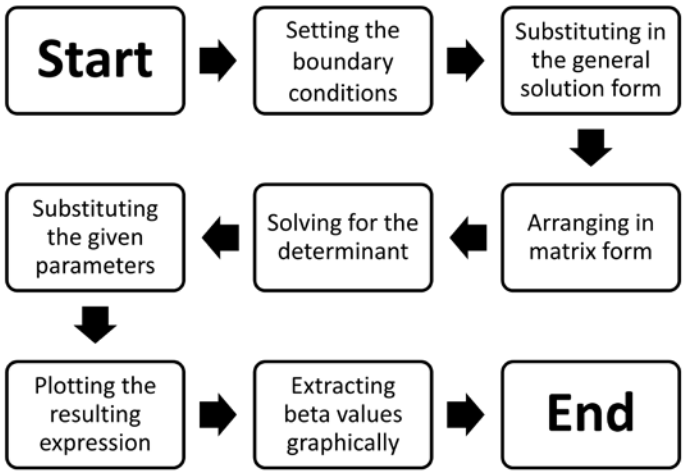

Figure 3. Eigenvalues calculating procedure.

For the presented beam system at Figure 2, the boundary conditions must be determined at the first pin support, the second pin support and at the free end from left to right. After substituting in the general form and arranging in matrix form gives the following matrix:

$$\begin{bmatrix} 0 & 1 & 0 & 1 & 0 & 0 & 0 & 0 \\ 0 & -1 & 0 & 1 & 0 & 0 & 0 & 0 \\ 0 & 0 & 0 & 0 & -\sin(\beta L) & -\cos(\beta L) & \sinh(\beta L) & \cosh(\beta L) \\ 0 & 0 & 0 & 0 & -\cos(\beta L)+\frac{\mu}{\rho A}\beta\sin(\beta L) & \sin(\beta L)+\frac{\mu}{\rho A}\beta\cos(\beta L) & \cosh(\beta L)+\frac{\mu}{\rho A}\beta\sinh(\beta L) & \sinh(\beta L)+\frac{\mu}{\rho A}\beta\cosh(\beta L) \\ \sin(\beta a) & \cos(\beta a) & \sin(\beta a) & \cosh(\beta a) & 0 & 0 & 0 & 0 \\ 0 & 0 & 0 & 0 & \sin(\beta a) & \cos(\beta a) & \sinh(\beta a) & \cosh(\beta a) \\ \cos(\beta a) & -\sin(\beta a) & \cosh(\beta a) & \sinh(\beta a) & -\cos(\beta a) & \sin(\beta a) & -\cosh(\beta a) & -\sinh(\beta a) \\ -\sin(\beta a) & -\cos(\beta a) & \sinh(\beta a) & \cosh(\beta a) & \sin(\beta a) & \cos(\beta a) & -\sinh(\beta a) & -\cosh(\beta a) \end{bmatrix} \begin{bmatrix} a_1 \\ a_2 \\ a_3 \\ a_4 \\ b_1 \\ b_2 \\ b_3 \\ b_4 \end{bmatrix} = \begin{bmatrix} 0 \\ 0 \\ 0 \\ 0 \\ 0 \\ 0 \\ 0 \\ 0 \end{bmatrix} \tag{2.2}$$

Solving for the determinant using Maple software, leads to the transcendental equation as follows:

$$\frac{1\rho A}{7}\Big(\Big(\Big(-28\,A\,\rho\,cosh(\beta a)^2-28\,A\,\rho\,cos(\beta a)^2+56\,\mu\,\beta\,sinh\,(\beta a)\,cosh\,(\beta a)-56\,\mu\,\beta\,sin\,(\beta a)\,cosh\,(\beta a)+56\;\rho\,A\Big)sinh\,(\beta L)+24\,\mu\,\beta\,cosh\,(\beta L)\,sinh\,(\beta a)\sin(\beta a)-28\cos(\beta L)\,(A\,\rho\cosh(\beta a)\sinh(\beta a)-A\rho\cos(\beta a)\sin(\beta a)+2\,\mu\,\beta\,cos(\beta a)^2-2\,\mu\,\beta)\Big)\sinh\,(\beta L)+28\Big(A\,\rho\,cosh\,(\beta a)sinh(\beta a)-A\,\rho\,cos(\beta a)\sin(\beta a)-\frac{8\;\mu\,\beta\cosh(\beta a)^2}{7}+\frac{8\;\mu\,\beta}{7}\Big)\cosh(\beta L)\sin(\beta L)+28\,A\Big(\big(\cosh(\beta a)^2\;cos(\beta L)-\cos(\beta a)^2\cos(\beta L)\big)\cosh(\beta L)+2\sinh\;(\beta a)\sin\;(\beta a)\big)\rho\Big)=0 \qquad (2.3)$$

Equation (2.3) can be solved to obtain the values of β since the values of ρ, a, A and μ are known for any beam system as shown in the coming section. After obtaining the values of β from Equation (2.3), the natural frequencies are calculated by Equation (2.4) [2].

$$f_n=\frac{\beta^2}{2\pi}\sqrt{\frac{EI}{\rho A}}\,[Hz] \qquad (2.4)$$

2.1.1 The Verification Model

In this section, a beam model with specific properties is analyzed using the analysis method in the previous sections to obtain the values of the natural frequencies for the first four eigenvalues and the first four mode shapes.

Table 1. The parameters of the validation model.

Parameter	Value
L	1 m
ρ	7850 kg/m^3
E	$2.05\cdot10^{11}$ N/m^2
μ	0.628 kg
I	$1.333\ 10^{-8}$ m^4
A	$4\cdot10^{-4}$ m^2
a	0.3 m

Since Equation (2.3) has infinite number of zeros and that the interest of this research is the first four modes, the parameters in Table 1 are substituted in Equation (2.3) and then it is plotted for a range of 4 π domain as follows:

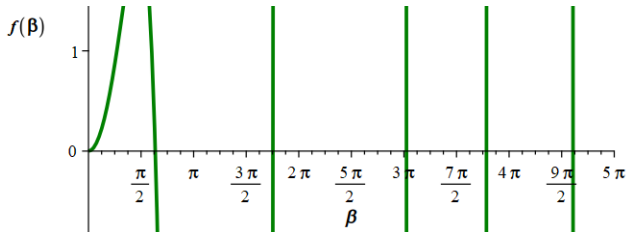

Figure 4. β values plot.

Then the zeros of the plot are extracted and substituted in Equation (2.4) to give the natural frequency values as listed in Table 2.

Table 2. Extracted β values and calculated natural frequencies.

β	Value	f_n $[Hz]$
1	1.99	18.72
2	5.52	143.25
3	9.53	426.33
4	11.85	659.5

To obtain the β values for different second pin support location, instead of repeating the previous step, a figure for calculating β values is obtained from Equation (2.3). For doing so, two variables are defined as follows, $\delta = \beta . l$ and $\lambda = a/l$. After rearranging and substituting them in Equation (2.3) then plotting the new expression for δ and λ yields to Figure 5. The curves in the plot correspond to the modes one to four from bottom to up respectively.

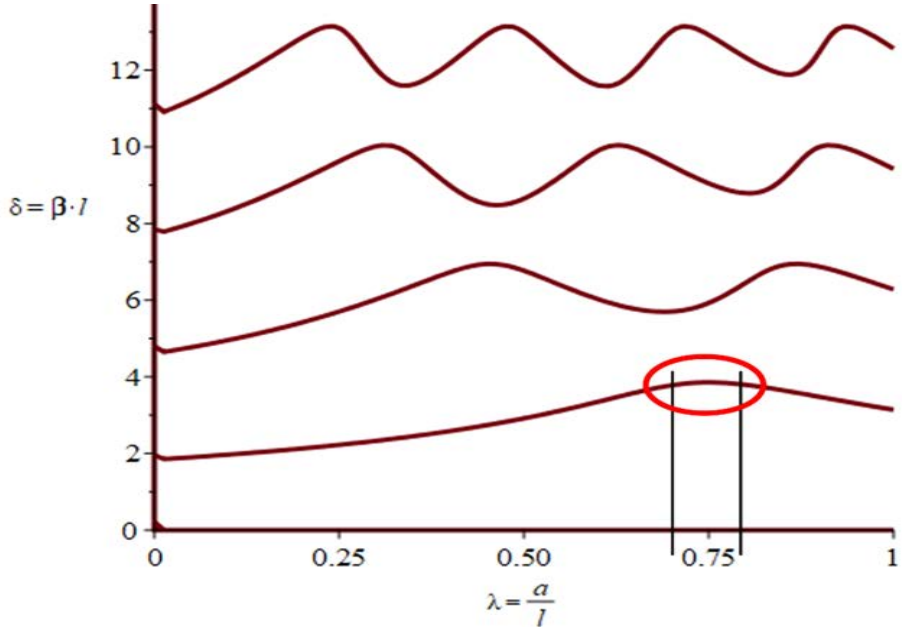

Figure 5. Eigenvalues for first 4 mode.

Figure 5 predicts the highest first natural frequency value to be near the a/l ratio of 0.75. To confirm this result, the following a/l ratios are analyzed.

Table 3. Frequency values.

a/l Ratio	Frequency $[Hz]$
0.1	13.9
0.2	16.1
0.3	18.8
0.4	22.6
0.5	27.9
0.6	35.8
0.7	47.3
0.8	58.4
0.9	55.2

As can be observed in Table 3, when the support is placed at the opposite end of the mass, the first natural frequency value is the lowest. As the a/l ratio increases, the first natural frequency value increases until the a/l ratio reaches 0.8. Beyond this point, the first natural frequency value decreases, confirming the findings from Figure 5. For the mode shapes, the boundary conditions equations are used in order to obtain relationships between the coefficients of the boundary conditions equations. The x axis represents the position along the beam system in meter and the y axis represents the normalized displacement.

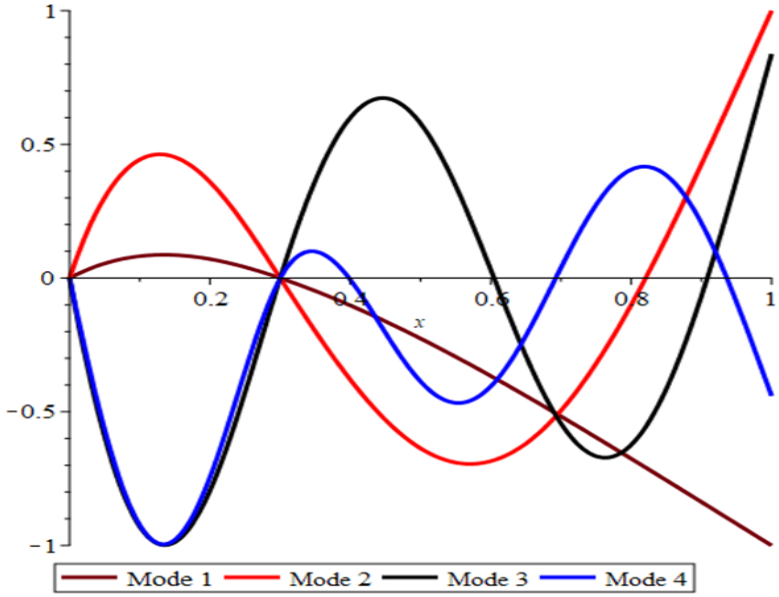

Figure 6. Proposed model mode shapes.

2.1.2 Conclusion

A study of a pinned-pinned-free beam with an attached mass at the free end utilized Euler-Bernoulli beam theory to derive a transcendental equation. This equation accommodates various pin support locations between the first pin and the free end, as well as different mass values. Eigenvalues were determined to calculate natural frequencies and mode shapes for model validation. The analytical model developed is applicable in engineering designs for structures such as crane arms, machine tool spindles, and boring bars.

2.2 Spindle Model Two: Timoshenko Beam Theory

This section aims to dynamically simulate a turning-center main spindle system using Timoshenko beam theory, applying the receptance coupling technique of systems to determine the first resonant frequency of the spindle under transverse vibrations. The results are validated using finite element analysis with ANSYS software.

2.2.1 Mathematical Modeling Principle

For the spindle system considered, the following assumptions are considered:

- the bearings are attached to a rigid frame,
- the transverse vibration of the spindle will also be assumed to be in a single plane.

The spindle may be broken down into several subsystems, such as shaft components and bearings, which can then be reassembled to form the entire spindle, as illustrated in Figure 7.

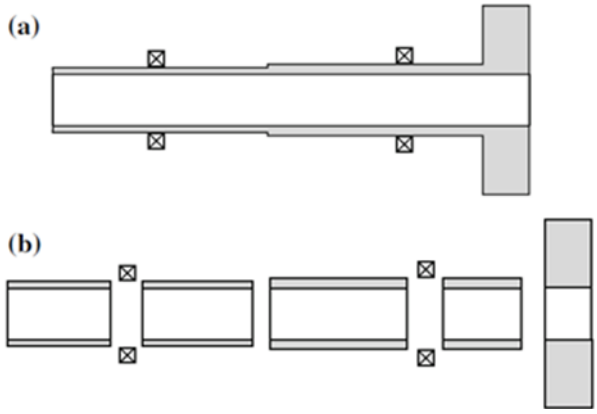

Figure 7. Typical spindle (a), subsystem component (b) [5].

Enforcing equilibrium and compatibility criteria at the joints is a part of the addition of the subsystems process. There are two coupling connections between each subsystem because the connected ends of each coupled ends of subsystem ends must have compatible displacement and slope due to bending for the transverse bending vibration of shafts.

2.2.2 Receptance Definition and Systems Addition

Receptance coupling simplifies vibrational energy flow analysis by modeling structures as subsystem combinations. Unlike traditional methods, it uses uncoupled mode matrices to assess displacement from external and boundary forces, considering damping and balancing energy transfers. The method integrates subsystems by combining their dynamic behaviors to predict overall displacement response. It aids in designing structures for optimal performance with minimal vibrations and predicts effects of subsystem changes on vibrational characteristics and energy distribution. Receptances, used in a systems approach, are defined as:

$$\boldsymbol{\alpha_{12}} = \frac{\boldsymbol{X_1 e^{i\omega t}}}{\boldsymbol{F_2 e^{i\omega t}}} = \frac{\boldsymbol{X_1}}{\boldsymbol{F_2}} \tag{2.5}$$

Where X_1 is the steady-state displacement response of a system at the position and in the direction specified by the subscript 1 and is oftenly a complex number that indicates a phase with respect to the steady exciting force $F_2 e^{i\omega t}$ that is applied to the system at the position and in the direction specified by the subscript 2. The receptance of shafts including shear and rotary inertia effects were derived by Potter and Stone [6] and Stone [7]. Also, the receptance of bearings was derived taking into consideration their stiffness. For adding systems, the process

consists of breaking the combined system A into its component systems, or subsystems B and C, and applying forces to each subsystem at coordinate 1, causing the separate systems to behave exactly as they would when they were combined as illustrated in Figure 8.

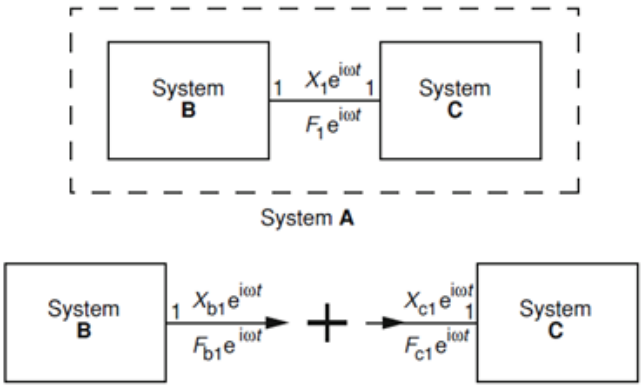

Figure 8. The addition of two subsystems [5].

2.2.3 The Validation Model

The spindle system illustrated in Figure 9. is analyzed using systems receptance coupling approach. The shaft elements and the chuck are modelled as hollowed circular sections while the workpiece is modelled as a cylinder.

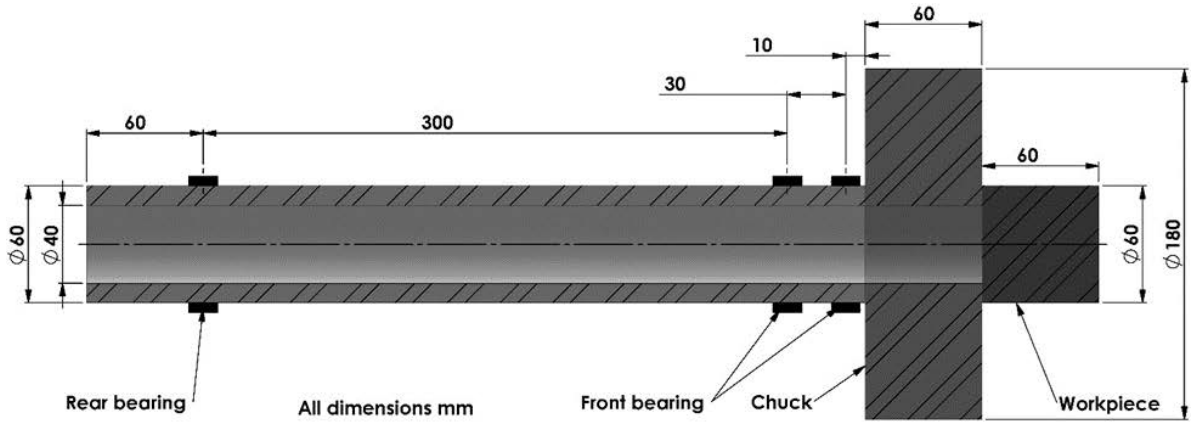

Figure 9. The spindle system including the subsystems and the related dimensions.

Figure 10. illustrates the block diagram of the spindle system including the shaft segments, the bearings, the chuck, and the workpiece. Symbols B, D and F represent the bearings, H represents the chuck, Symbol I represents the workpiece and the rest of the subsystems represent the shaft segments. The used material of the spindle is assumed to be ASTM A36 steel. The stiffness of the bearing used in the analysis is $7.5 \cdot 10^8$ N/m [5].

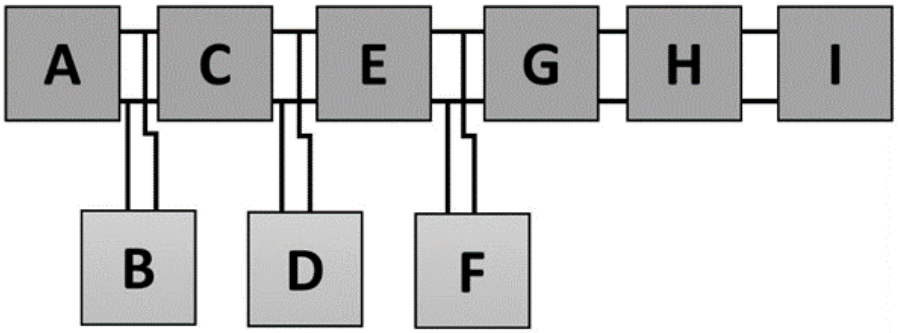

Figure 10. Addition of shaft and bearing subsystems.

2.2.4 Results

A code utilizing systems receptance coupling approach for analyzing the spindle system presented in Figure 9. is written to obtain the response of the system over a frequency range of 800 Hz as illustrated in Figure 11, the values of the first resonant frequency can be extracted.

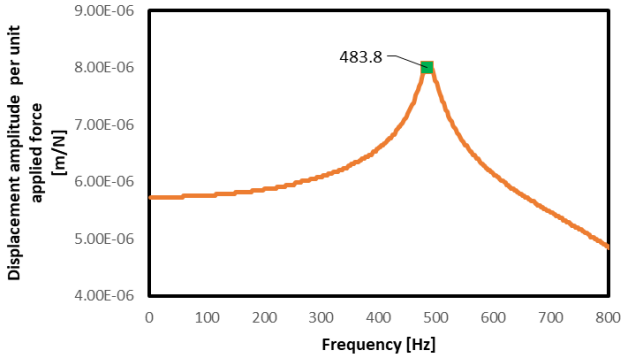

Figure 11. Displacement amplitude per applied force response of the proposed spindle system.

Finite element modal analysis of the proposed model is performed using ANSYS V19 software to compare the result of the first natural frequency value.

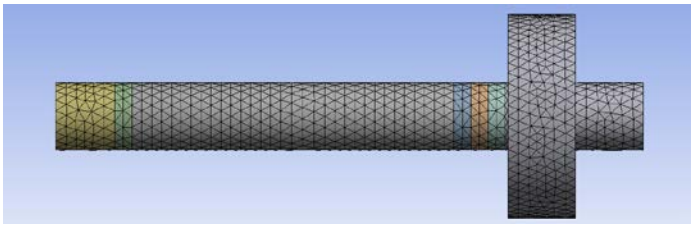

Figure 12. The meshed spindle system.

Figure 13. shows the first resonant frequency mode shape obtained from ANSYS 19.

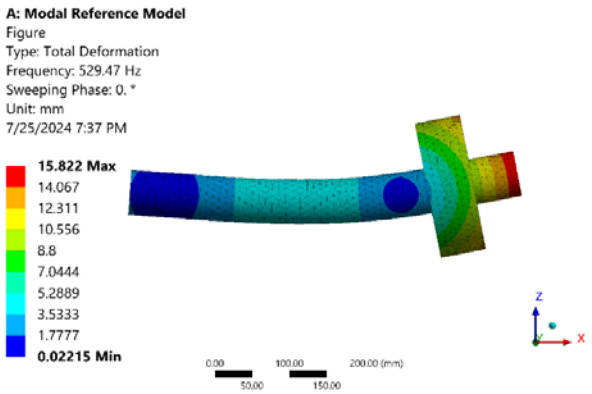

Figure 13. ANSYS 19 spindle system mode shape.

Table 4 compares the results of first resonant frequency [Hz] of the spindle system using the systems receptance; coupling approach and the results from the finite element analysis using ANSYS software.

Table 4. Results comparison.

Mode number	Receptance approach	ANSYS	Error %
1	483.3 Hz	529.47 Hz	8.7%

2.2.5 Conclusion

A spindle system supported by three bearings is analyzed using the receptance coupling approach of systems, considering the stiffness of the bearing to determine the first resonant frequency. The same spindle system is also analyzed using the finite element method (FEM) with ANSYS software. A comparison of the results reveals good agreement in the resonant frequencies. The code used to analyze the spindle system with the receptance coupling approach can be modified to account for varying bearing stiffness, different bearing locations, and changes in the lengths and diameters of the shaft segments, as well as the chuck and workpiece.

3 OPTIMIZATION AND RESULTS

3.1 Introduction

The chapter aims to improve a lathe spindle performance by focusing on the reduction of chatter and enhancement of stress capacity, all while keeping the overall mass of the system unchanged. The design optimization will be implemented through two specific methods.

1. The Kuhn-Tucker optimality criterion with the Grapho-Analytical technique.
2. The RSM (Response Surface Methodology) and ANOVA (Analysis of Variance) as they are complementary methods used in statistical analysis and experimental design.

By employing these two approaches, the aim is to identify and implement structural modifications that can effectively optimize the lathe spindle system.

3.2 The Proposed Spindle System Design and Analysis

The proposed model of the lathe spindle consists of a shaft of uniform thickness, three bearings, a chuck, and a workpiece. Figure 14 shows a section view of the model.

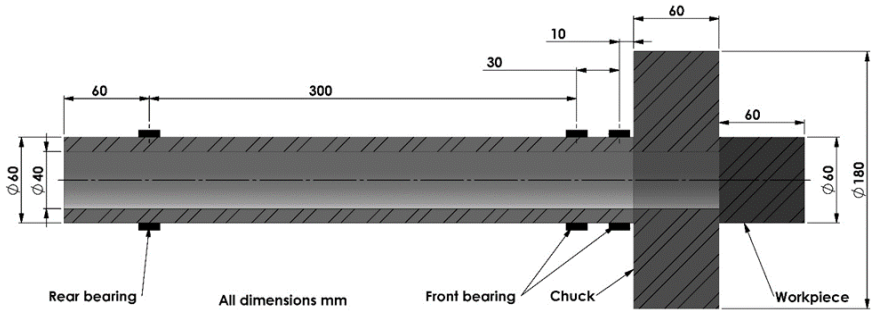

Figure 14. Section View of Lathe Spindle Proposed Model.

The main reason for selecting this model is that it is used in the literature in [5] and in [4]. Therefore, it can serve as a good reference model. Some limits for the optimization are taken into. First, the minimum inner diameter of the shaft should not be less than 40 mm, as this is necessary for the bar feeding mechanism. Additionally, the shaft thickness must not be less than 7 mm, considering the maximum allowable angle of twist is 0.25 degree/meter [8]. The torque applied to the spindle is 576 Nm (Based on the data sheet of Haas ST-35L CNC lathe [9]). Finally, the assumed bearing stiffness is $7.5 \cdot 10^8$ N/m [5].

3.3 The Grapho- Analytical Optimization Method

The grapho-analytical method identifies the optimal point where the iso-line of the objective function tangentially intersects the feasible region, which may occur at a border or corner point. This method is classified into two strategies: the graphical approach, which uses diagrams to depict iso-lines, and the analytical approach, which employs algebraic techniques to derive precise optimum values from the constraints and objective function.

3.3.1 The Optimization of the Proposed Model (Graphically)

Establishing the optimization system involves two primary steps. First, setting the constraints of the optimization problem. Second, defining the objective function and its contours.

3.3.1.1 The first set of parameters

For the proposed model, the goal is to increase the inner diameter of the shaft near the chuck while reducing its thickness to maintain the overall shaft mass. The idea behind the proposed model in terms of rigidity and strength is the following:

- Uniform Shaft: A uniform shaft maintains the same diameter and shape across its length, ensuring consistent cross-sectional area and moment of inertia.

- The tapered shaft design, characterized by an increasing diameter towards the chuck and a compensating thinner wall, results in a variable cross-sectional area and moment of inertia. This configuration enhances rigidity near the chuck, where the larger diameter provides superior resistance to bending and torsion in areas subjected to higher machining forces.

Two variables are introduced that relate to each other through by the pre-optimized shaft system volume is 628318.53 mm^3. The variables are the bigger radius of the cone, denoted R, and the cone thickness, denoted t. Figure 15 illustrates the truncated hollow cone under consideration.

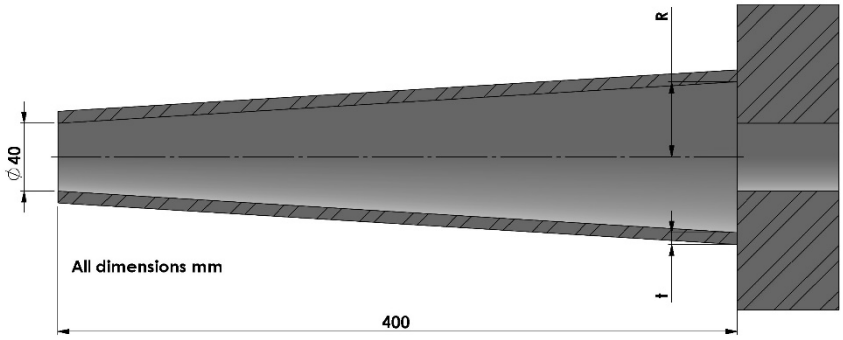

Figure 15. Section view of the truncated Hollow Cone Representation for Optimizing Spindle Shaft Design.

The relationship between the variables is derived from the volume equation and is presented in Equation (3.1).

$$\boldsymbol{Volume} = \left(\frac{\pi L}{3}\left((\boldsymbol{R}+\boldsymbol{t})^2 + (\boldsymbol{27.5}+\boldsymbol{t})^2 + (\boldsymbol{R}+\boldsymbol{t}) + (\boldsymbol{27.5}+\boldsymbol{t})\right)\right) - (\frac{\pi L}{3}\left(\boldsymbol{R^2} + \boldsymbol{27.5^2} + \boldsymbol{27.5R}\right)) \xrightarrow{\boldsymbol{yields}} \quad \boldsymbol{R} = -\frac{(\boldsymbol{t}+\boldsymbol{34.5})(\boldsymbol{t}-\boldsymbol{14.5})}{\boldsymbol{t}} \tag{3.1}$$

Additional constraints are introduced as follows:

$$\boldsymbol{R} \geq \boldsymbol{20\ mm} \tag{3.2}$$

$$\boldsymbol{7\ mm} \leq \boldsymbol{t} \leq \boldsymbol{10\ mm} \tag{3.3}$$

The spindle system was analyzed using the Finite Element Method in ANSYS V19 to determine the first natural frequency for various values of R and t. The findings, summarized in Table 5, facilitated the creation of an objective function through a second-degree polynomial fitting of t and frequency values, expressed in Equation (3.4).

Table 5. t and frequency values used to establish the objective function equation.

t [mm]	R [mm]	Frequency [Hz]
7.00	44.46	324.52
7.25	41.75	323.30
7.50	39.20	321.91
7.75	36.79	320.43
8.00	34.53	318.80

$$R(t) = -1.04t^2 - 9.876t + 306.35 \quad (3.4)$$

The optimization process is visualized in Figure 16, which shows a plot of the objective function and its contours alongside the implicit and explicit constraints.

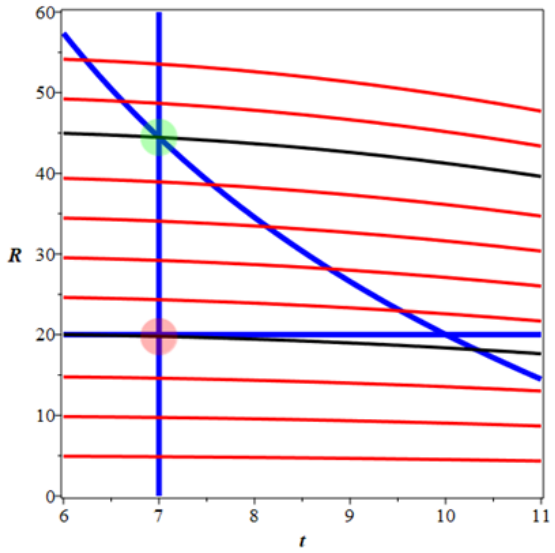

Figure 16. The plot of the thickness and diameter next to the chuck constraints and the objective function contours of the first natural frequency.

In Figure 16, the feasible solution region is defined by the area between the constraint borders represented by blue lines and a curve. The contours of the objective function are illustrated by red curves, while optimal objective function contours are depicted in black. The green circle marks the optimal point, determined by the intersection of two constraints and an objective function contour, with values of t at 7 mm and R at 44.46 mm. This configuration yields the maximum first natural frequency. The red point indicates the minimum optimal point.

3.3.1.2 The second parameter, the rear bearing location

The second parameter is to investigate the location of the rear bearings, the main steps of the previous section are repeated in order to construct the objective function. For the constraints, the first constraint is the axial location of the bearing taking the left end of the shaft as a reference, then the constraint of the axial location of the bearing is expressed as:

$$7.5\ mm \leq L \leq 200\ mm \quad (3.5)$$

The axial location range starts at 7.5 mm, as this is the bearing center, and ends at 200 mm, the shaft midpoint. Another constraint is the relationship between the axial location and the radius of the shaft associated with each axial location. This relationship is expressed as:

$$D = 0.0612L + 20 \quad (3.6)$$

To establish the objective function, the spindle system is analyzed using the Finite Element Method using *ANSYS V19* software for a range of R and L values to determine the first natural frequency. Table 6 lists the values of L and frequency used to establish the objective function by fitting D and frequency values in a third-degree polynomial which is Equation (3.7).

Table 6. L and frequency values used to establish the objective function equation.

L[mm]	D[mm]	Frequency [Hz]
7.5	20.46	712.16
50	23.06	767.71
100	26.12	819.04
150	29.18	850.01
200	32.24	826.90

$$\boldsymbol{D(L) = \left(-0.3 * 10^{-5}\right)L^3 - 0.0027L^2 - 1.1843L + 703.62} \quad (3.7)$$

The optimization process is visualized in Figure 17.

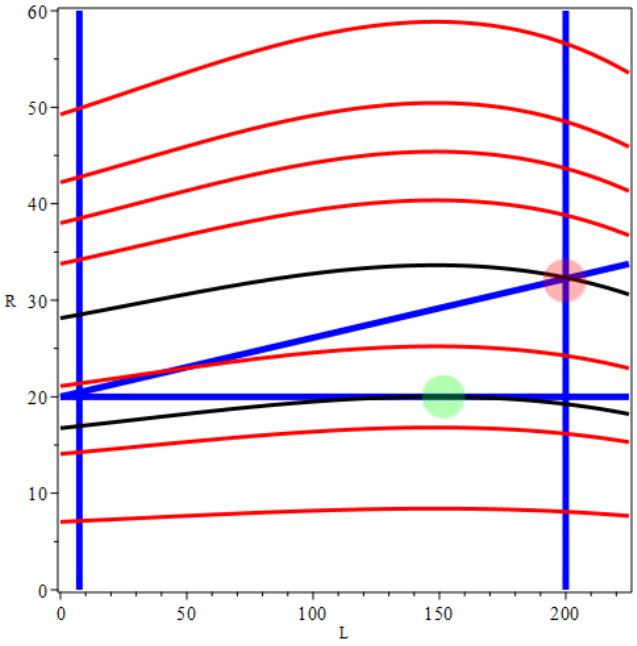

Figure 17. The plot of the rear bearing location constraints and the objective function contours of the first natural frequency.

In Figure 17, the feasible solution region is represented by the enclosed area between the blue lines denoting constraint borders. The red curves depict objective function contours. The black curves represent optimal objective function contours. The green circle indicates the optimal point (maximum point), as it is tangent to the feasible region. This implies that when the two curves are equal, there is only one solution where they intersect. At the green circle, L value is 162 mm. This implies the highest first natural frequency occurs when the rear bearing center is located 162 mm from the shaft left end. The red point is an optimal point representing the minimum.

3.3.2 The Optimization of the Proposed Model (Analytically)

The confirmation of the results of the graphical solution should be ensured by the analytical solution. To optimize the spindle system for the value of the first natural frequency through analytical means, an implicit constraint Equation should be set equal to the objective function Equation after being multiplied by a factor "C" responsible for shaping the contours of the objective function. Equation (3.8) represents the outcome of this process.

$$-\frac{(t+34.5)(t-14.5)}{t} = (-1.04t^2 - 9.876t + 306.35) * C \quad (3.8)$$

In the analytical solution, the primary objective is to obtain a single solution of Equation (3.8) for the variable "t" within the domain of 7 to 10 mm that at the same time intersects with the constraint vertical line at x =7. To achieve this goal, an algorithm has been devised and depicted in Figure 18, which aids in determining the optimal solution.

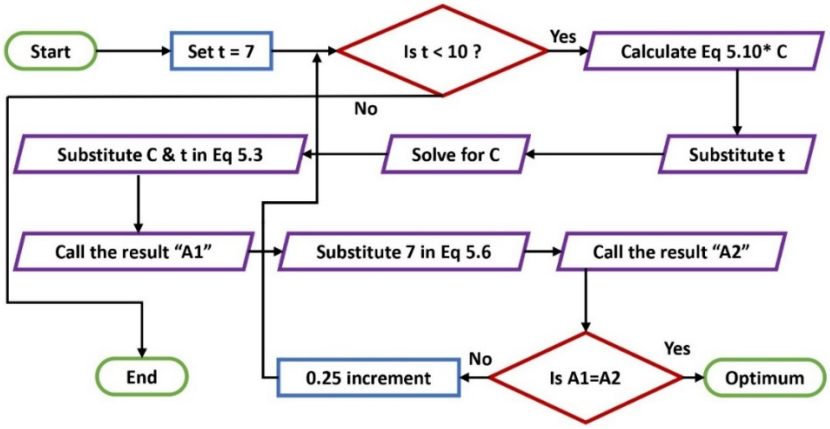

Figure 18. The optimum solution finding algorithm.

After performing the solution, the value of C is 0.137 and the corresponding t value is 7 mm. Based on Equation (3.8) the value of R is 44.46 mm which matches the result of the graphical method.

3.4 RSM and ANOVA Optimization

RSM and ANOVA are often used together since RSM: Provides a model and optimization pathway by systematically varying input variables and analyzing their effects. Also, ANOVA identifies which variables and interactions are statistically significant, refining the RSM model and focusing the optimization efforts [10]. RSM is employed to develop an empirical model that characterizes the relationship between key parameters (shaft geometry and bearing location) and the natural frequency response of the system. This modeling is accomplished through statistically designed experiments and regression analysis [11]. ANOVA enables the determination of the statistical significance of individual parameters and their interactions on the frequency response [12]. Taken together, RSM allows the complex relationships between

inputs and response to be modeled, while ANOVA highlights the most critical factors [13]. This approach enables the systematic optimization of parameters to maximize natural frequency and chatter reduction within operational constraints.

3.4.1 The Optimization of the Proposed Model (First Natural Frequency Value)

Design expert software is employed to run the analysis and generate response surfaces.

3.4.1.1 Stage Number One, Optimizing the Rear Bearing Location

The ranges of the factors selected are the same ranges mentioned in the Grapho – analytical technique as the main goal is to compare the results of the RSM and the Grapho – analytical technique.

1. Conducting the experiment:

   The experiments of Table 7 are conducted using *ANSYS V19* software in order to establish the required data to run the *ANOVA* analysis and to generate the response surface.

Table 7. Runs used to construct the response surface 1

RUN	Factor 1 A: Radius [mm]	Factor 2 B: Rear bearing location [mm]	Response 1 Frequency [Hz]
1	32.2	32.3	642.7
2	20	7.5	506.2
3	32.2	103.7	706.1
4	44.4	7.5	712.1
5	20	200	612.0
6	14.9	103.7	488.9
7	32.2	239.8	654.4
8	44.4	200	826.9
9	49.5	103.7	860.9

Figure 19 illustrates the response surface for optimizing rear bearing location.

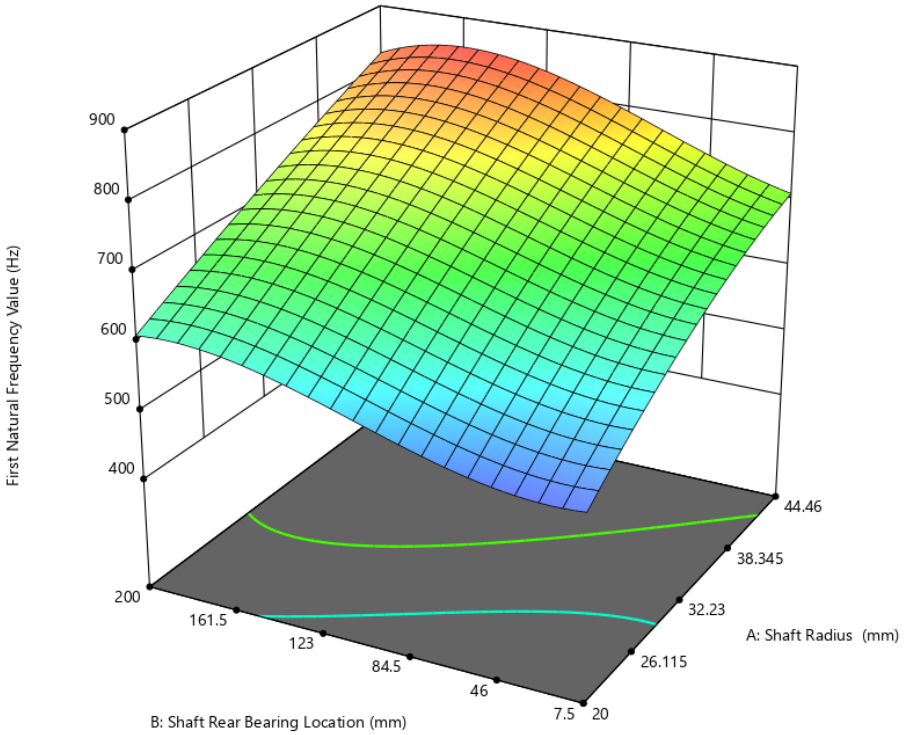

Figure 19. The response surface of optimizing the rear bearing location.

As observed in Figure 19, the surface height peaks (red zone) when the shaft radius next to the chuck is 44.46 mm and the rear bearing location ranges from 155-165 mm from the shaft end.

3.4.1.2 Stage Number Two, Optimizing the Geometry of The Shaft

The same steps of section 5.4.1.1 are repeated in this section taking into consideration the different runs for constructing the response surface as listed in Table 8.

Table 8. Runes used to construct the response surface 2

RUN	Factor 1 A: Thickness of the shaft [mm]	Factor 2 B: Radius [mm]	Response 1 Frequency [Hz]
1	8.5	32.23	676.821
2	10	20	535.424
3	7	20	448.772
4	8.5	49.5258	692.912
5	7	44.46	760
6	8.5	14.9342	406.017
7	6.37868	32.23	760
8	10.6213	32.23	747.674
9	10	44.46	586.935

Figure 20 illustrates the response surface for optimizing shaft geometry.

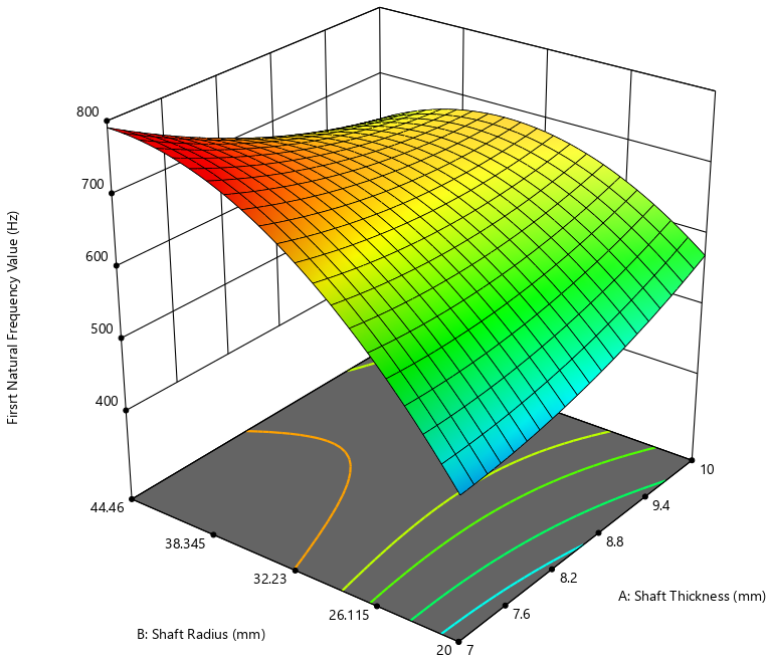

Figure 20. The response surface of optimizing the geometry of the shaft.

As observed in Figure 20, the response surface height peaks when the shaft radius next to the chuck is 44.46 mm and shaft thickness is 7 mm.

3.4.1.3 Comparison of the Results of the Two Optimization methods

In this subsection, a comparison of the results of the two optimization methods is carried out. Table 9 lists the optimization methods and their results.

Table 9. Comparison of Optimization Methods and Their Corresponding Natural Frequencies.

Parameter / Method	Optimized R [mm]	Optimized t [mm]	Optimized L [mm]	1st Natural Frequency [Hz]
The Grapho- Analytical Method	44.46	7	162	-
RSM and ANOVA Method	44.46	7	161	792

The Grapho-Analytical Method provides optimized parameters—namely, a radius of the shaft next to the chuck of 44.46 mm, a thickness of the shaft of 7 mm, and a rear bearing location of 162 mm—aimed at achieving an optimal first natural frequency. However, it does not directly yield the value of this frequency. Instead, these parameters are intended for use with further methods, such as Finite Element Analysis (FEA), to determine the actual first natural frequency. On the other hand, the RSM and ANOVA Method not only delivers optimized parameters but also estimates the first natural frequency to be 792 Hz. This estimate provides a useful indication but is not the final value. For precise frequency determination, FEA is necessary, which, in this case, reveals the actual first natural frequency to be 852.52 Hz as indicated in the next subsection. This result suggests that while the RSM and ANOVA Method

offers a close approximation, FEA is essential for accurate validation and refinement of the natural frequency predictions.

3.5 Results Evaluation

The optimization results are evaluated and compared to the non-optimized model. Figure 21 illustrates the non-optimized and optimized models, including geometrical dimensions.

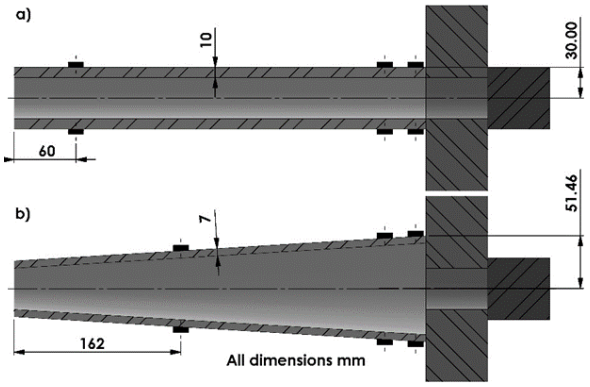

Figure 21. a) The non-optimized model, b) The optimized model.

As shown in Figure 22, the first natural frequency of the optimized model is 323.05 Hz higher than the non-optimized model, representing a 60.5% increase.

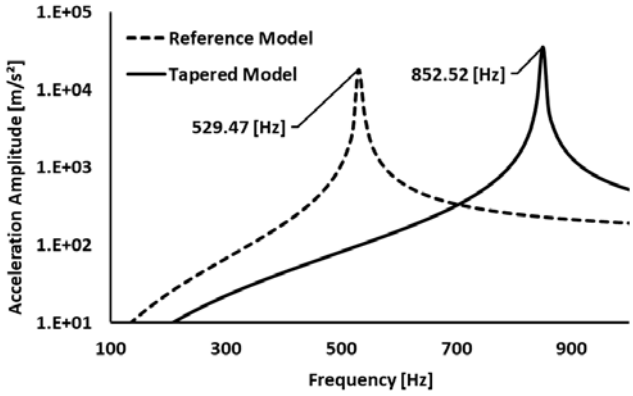

Figure 22. Frequency response of the optimized and the non-optimized models.

A 15.375 kN load is applied to the non-optimized model workpiece to better understand the optimized enhanced stress capacity of the model. This load was chosen because it causes permanent spindle system deformation. The optimized model is then subjected to the same load. Figure 23 illustrates the boundary conditions as well as the results of applying this load to optimized and non-optimized models.

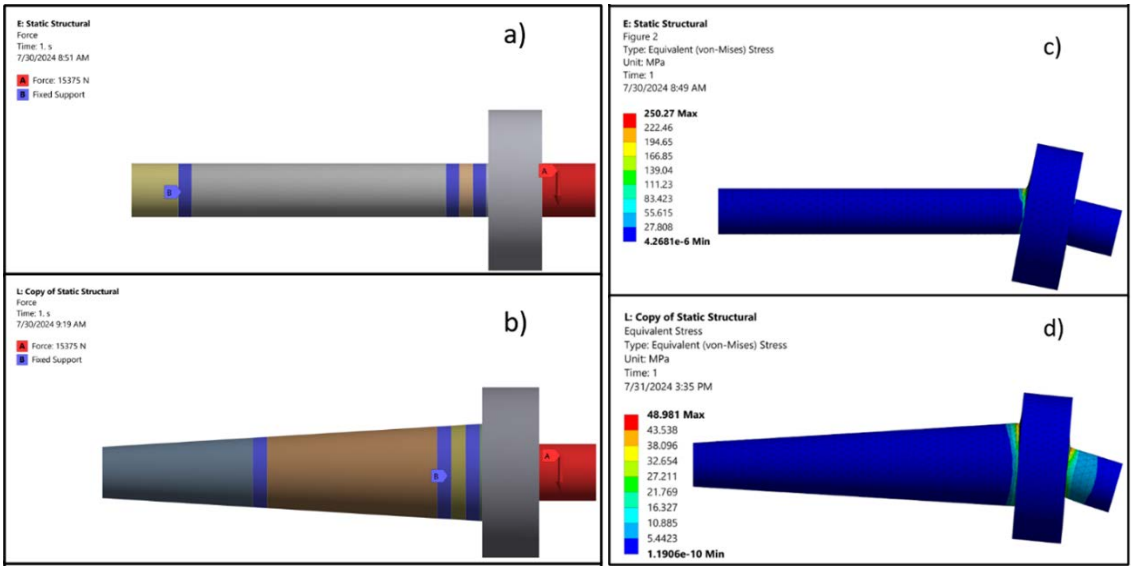

Figure 23. a) the reference spindle model boundary conditions, b) the proposed spindle model boundary conditions, c) the deformation stress analysis result, the reference model, d) the deformation stress analysis result, the proposed spindle model.

As observed in Figure 23, a relatively large enhancement in stress capacity is achieved after optimization. In summary, Table 10 compares the optimized and non-optimized models.

Table 10. Model Performance Comparison: Optimized and Non-Optimized Models.

Property / Model	Stress [MPa]	1st Natural frequency [Hz]
Non-optimized	250	529.47
Optimized	48.98	852.52
Enhancement [%]	411	61.01

3.6 The Effect of The Stiffness of The Rear Bearing

Bearing preload is a key factor in governing the stiffness of the bearings which can be increased by changing the preload applied to it. This is applicable to an optimum level after which the stiffness of the bearing reduces with additional preload [14]. This section investigates the effects of increasing the rear bearing stiffness value in relation to the optimum location of the bearing. The rear bearing stiffness value is increased by 10%, and the same analysis is repeated to investigate how the optimum location of the rear bearing location changes, as well as the value of the first natural frequency.

Table 11. The effect of the rear bearing stiffness on its location and the first natural frequency value.

Bearing stiffness [N/m]	Optimum rear bearing location [mm]	Frequency [Hz]
$7.50 \cdot 10^8$	162	850.75
$8.25 \cdot 10^8$	167	855.43
$9.00 \cdot 10^8$	169	858.12
$9.75 \cdot 10^8$	171	860.41

3.7 Application To a Real Case

The authors of [15] investigated the vibration resistance of CNC lathe machine tools in an operational production environment. Using impact testing, they measured the dynamic characteristics and frequency response functions of the spindle units on multiple machines. Because the geometry of the analyzed spindle, as well as the stiffness values of the bearings, are available, it was used as a case study to apply the optimization introduced earlier in this chapter. Figure 24 illustrates the spindle unit described in [15].

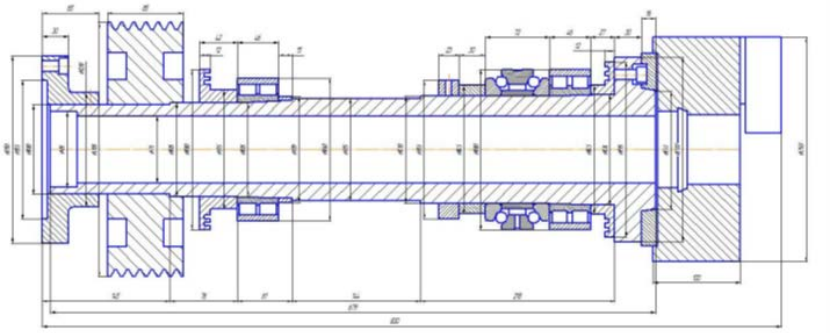

Figure 24. Spindle unit of machine tool.

The 3D geometry of the spindle unit was created using Figure 24. The remodeled geometry is illustrated in Figure 25.

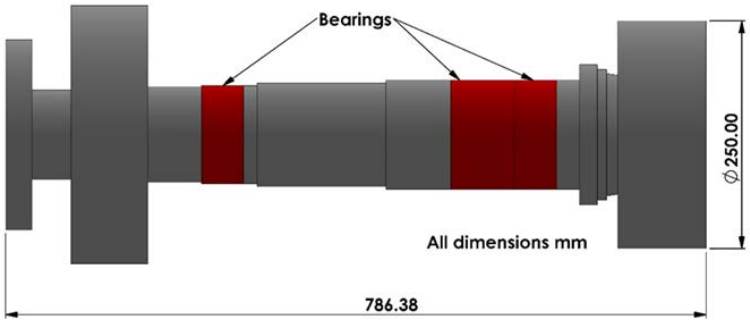

Figure 25. The remodeled geometry.

Figure 26 a) illustrates the results of the spindle unite impact testing in [15]. The blue curve is the more of interest because the values of the stiffness of the spindle bearings are available in [15]. Figure 26 b) shows the result of the modal finite element analysis of the remodeled spindle unite. The error in the first frequency value is 0.8%.

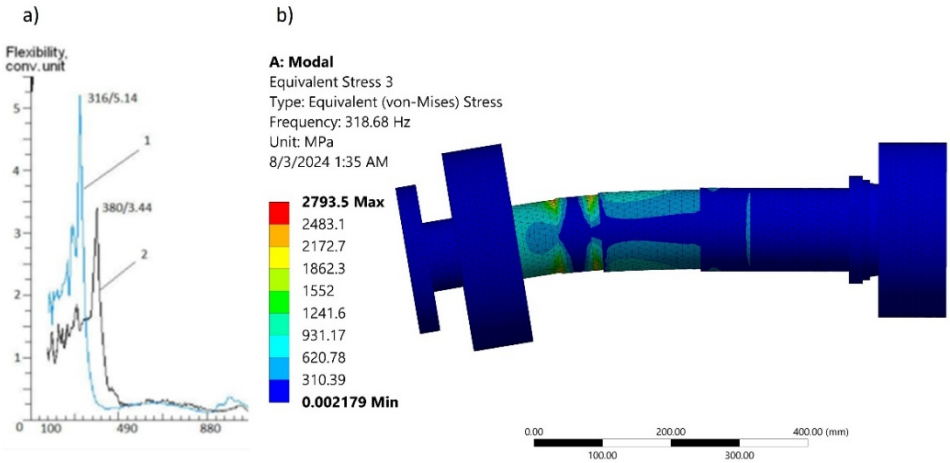

Figure 26. The results of the impact testing in [10], b) The modal analysis result of the remodeled spindle.

The mass of the mentioned system is 68.18 kg when only the spindle shaft and the chuck are considered. The thickness of the shaft of the equivalent spindle system is 13.5 mm after repeating the optimization process described in this chapter. The radius of the shaft next to the chuck is 96.41mm. The optimized rear bearing location is 216.48 mm measured from the free end of the shaft as illustrated in figure 27 b) while it was 243.53 mm in the model of [15].

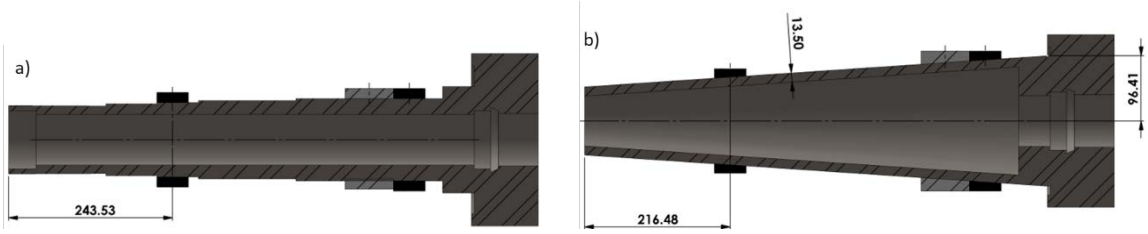

Figure 27. a) The remodeled spindle unite in [10], b) The optimized spindle unite.

Figure 28 a) illustrates the finite element method analysis of the model presented in [15], The first natural frequency value is 487.75 Hz, as well as the mode shape. Figure 28 b) illustrates the optimized finite element method analysis of the model, which reveals that the first natural frequency value is 561.63 Hz, along with the mode shape.

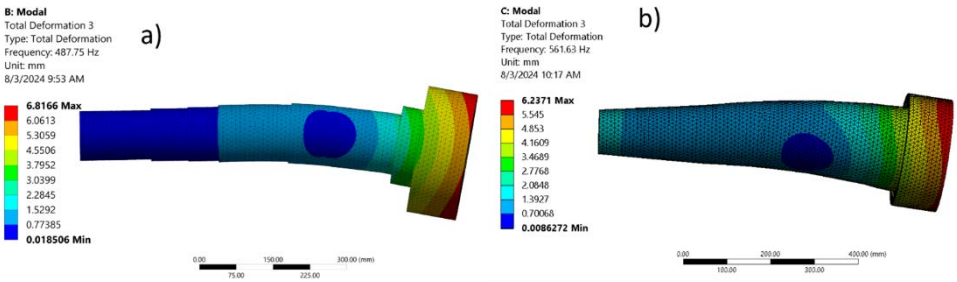

Figure 28. a) The modal analysis result of the remodeled spindle unite in [15], b) The modal analysis result of the optimized spindle unite.

The optimized spindle model shows a 15% increase in the first natural frequency value.

4 THESES

4.1 Thesis One

I proved that transforming the geometry of a horizontal lathe machine spindle shaft from a uniform to a conical shape—increasing its diameter towards the chuck and reducing its thickness—significantly improves the vibrational performance of the spindle system. This modification, achieved while maintaining the overall mass and length of the spindle constant. The result is a notable enhancement in the natural frequency of the spindle system, leading to a reduced likelihood of machining chatter and indicating superior stability and precision in machining operations

Related publications: **MA1, MA2 and M4**

4.2 Thesis Two

I proved that strategic optimization of the rear bearing location within a horizontal lathe machine spindle system plays a significant role in enhancing its vibrational characteristics. Through the finite element method, this optimization was identified as a pivotal factor in improving the natural frequency of the spindle, thereby bolstering its resistance to machining chatter. This consideration, in conjunction with the geometric modifications to the spindle shaft, highlights a comprehensive approach to improving the dynamic performance of machining equipment.

Related publications: **MA1 and MA2**

4.3 Thesis Three

I proved that, within a horizontal lathe machine spindle system, there exists a direct positive correlation between the stiffness of the rear bearing and the first natural frequency of the spindle system. Additionally, the stiffness of the rear bearing influences its optimum placement for achieving the highest possible first natural frequency of the spindle system. This discovery unveils the intricate interplay between bearing stiffness and its positioning, shedding light on a crucial aspect of spindle design that directly impacts machining stability and efficiency. By optimizing both the stiffness and the location of the rear bearing, this research contributes a significant advancement towards refining spindle systems for enhanced performance.

Related publications: **MA1**

4.4 Thesis Four

The derived expression for calculating the natural frequencies and plotting the mode shapes of a simply-supported beam with an overhang mass, validated by finite element analysis, allows for optimizing the point mass and support location without requiring complex analysis. This approach significantly enhances the performance of systems such as machine tool spindles and boring bars by providing a more efficient method for determining their dynamic characteristics.
Related publications: **MA5**

5 LIST OF PUBLICATIONS RELATED TO THE TOPIC OF THE RESEARCH FIELD

MA1. Mohammed, Alzghoul; Sarka, Ferenc; Szabó, Ferenc János, Optimization of spindle system first natural frequency values using response surface methodology of variance, VOSTOCHNO-EVROPEISKII ZHURNAL PEREDOVYKH TEKHNOLOGII / EASTERN- EUROPEANJOURNAL OF ENTERPRISE TECHNOLOGIES1 : 1pp. 17-25. , 9 p. (2025).
DOI: https://doi.org/10.15587/1729-4061.2025.320497

MA2. Alzghoul, Mohammad; Sarka, Ferenc; Szabó, Ferenc János, Improving Chatter Performance of a Lathe Spindle through Grapho-Optimization, DESIGN OF MACHINES AND STRUCTURES13 : 2pp. 5-12. , 8 p. (2023)
DOI: https://doi.org/10.32972/dms.2023.012

MA3. Alzghoul, Mohammad; Sarka, Ferenc; Szabó, Ferenc J.,Analytical and Experimental Techniques for Chatter Prediction, Suppression and Avoidance in Turning: Literature Survey, DESIGN OF MACHINES AND STRUCTURES12 : 2pp. 33-43. , 11 p. (2022)
DOI: https://doi.org/10.32972/dms.2022.011

MA4. Alzghoul, Mohammad; Sarka, Ferenc; Szabó, Ferenc J., A Spindle System Analysis Using Systems Receptance Coupling Approach, DESIGN OF MACHINES AND STRUCTURES12 : 2pp. 25-32. , 8 p. (2022)
DOI: https://doi.org/10.32972/dms.2022.010

MA5. Alzghoul, Mohammad; Cabezas, Sebastian; Szilágyi, Attila, Dynamic modeling of a simply supported beam with an overhang mass, POLLACK PERIODICA: AN INTERNATIONAL JOURNAL FOR ENGINEERING AND INFORMATIONSCIENCES17 : 2pp. 42-47. , 7 p. (2022)
DOI: https://doi.org/10.1556/606.2022.00523

MA6. Al-zgoul, Mohammad; Szilágyi, Attila, DYNAMICAL SIMULATION OF A CNC TURNING CENTER,DESIGN OF MACHINES AND STRUCTURES10 : 2pp. 91-96. , 6 p. (2020)
DOI: https://doi.org/10.32972/dms.2020.019

MA7. Al-zgoul, Mohammad; Szilágyi, Attila, DYNAMICAL SIMULATION OF A CNC TURNING CENTER (SURVEY PAPER). DESIGN OF MACHINES AND STRUCTURES10 : 2pp. 85-90. , 6 p. (2020)
DOI: https://doi.org/10.32972/dms.2020.018

6 REFERENCES

[1] C. L. Lida Zhu, "Recent progress of chatter prediction, detection and suppression in milling," *Mechanical Systems and Signal Processing,* vol. 143, 2020.

[2] J. Hong, J. Dodson, S. Laflamme and A. Downey, "Transverse Vibration of Clamped-Pinned-Free Beam with Mass at Free End," *Applied Sciences,* vol. 9, no. 15, pp. 2996-3012, 2019.

[3] S. C. A. S. Mohammad Alzghoul, "Dynamic modeling of a simply supported beam with an overhang mass," *Pollack Periodica,* vol. 14, no. 2, p. 42–47, 04 May 2022.

[4] A. P. B. J. S. o. c. P. 1. t. a. r. d. R J Lambert, "Some characteristics of rolling-element bearings under," *Proceedings of the Institution of Mechanical Engineers, Part K: Journal of Multi-body Dynamics,* vol. 220, no. 3, pp. 157-170, 2006.

[5] B. Stone, Chatter and Machine Tools, Perth: Springer, 2014.

[6] S. B. Potter SJ, "The calculation of the response of spindle-bearing systems to oscillating forces.," MTIRA research report, 1974.

[7] S. BJ, "The receptances of beams, in closed form, including the effects of shear and rotary inertia.," *Proc IMechE,* vol. 206, no. 2, pp. 87-94, 1992.

[8] Z. Árpád, Gépelemek I, Budapest: Nemzeti Tankönyvkiadó, 1999.

[9] [Online]. Available: https://www.haas.co.uk/lathes/st-35l/. [Accessed 20 04 2023].

[10] D. C. Montgomery, Design and Analysis of Experiments, John Wiley & Sons, 217.

[11] D. C. M. C. M. A.-C. RAYMOND H. MYERS, Response surface methodology: process and product optimization using designed experiments, John Wiley & Sons, 2016.

[12] B. İ. H. Bas Deniz, "Modeling and optimization I: Usability of response surface methodology," *ournal of Food Engineering,* vol. 78, no. 3, pp. 836-845, 2007.

[13] A. I. M. S. Khuri, "Response surface methodology," *WIREs Computational Statistics,* vol. 2, no. 2, pp. 128-149, 2010.

[14] T. Harris and M. Kotzalas, "Essential Concepts of Bearing Technology," in *Rolling Bearing Analysis*, New Yourk, Taylor & Francis Group, 2006, pp. 119-128.

[15] F. S. a. N. K. a. S. Shemyakin, "Operational Assessment of Machine Tool Vibration Resistance," *Procedia Engineering,* vol. 150, pp. 215-219, 2016.